

Article

Improving the Voltammetric Determination of Hg(II): A Comparison Between Ligand-Modified Glassy Carbon and Electrochemically Reduced Graphene Oxide Electrodes

Matei D. Raicopol ¹, Andreea M. Pandele ¹, Constanța Dascălu ², Eugeniu Vasile ¹, Anamaria Hanganu ³ , Gabriela-Geanina Vasile ⁴ , Ioana Georgiana Bugean ¹, Cristian Pirvu ¹ , Gabriela Stanciu ^{5,*} and George-Octavian Buica ^{1,*}

¹ Faculty of Applied Chemistry and Materials Science, University Politehnica of Bucharest, 1-7 Gheorghe Polizu St., 011061 Bucharest, Romania; m_raicopol@chim.upb.ro (M.D.R.); madalina.pandele@upb.ro (A.M.P.); eugeniu.vasile@upb.ro (E.V.); ioana.g.lazar@gmail.com (I.G.B.); cristian.pirvu@upb.ro (C.P.)

² Faculty of Applied Sciences, University Politehnica of Bucharest, 313 Splaiul Independenței, 060042 Bucharest, Romania; constanta_dascalu@physics.pub.ro

³ Department of Organic Chemistry, Biochemistry and Catalysis, University of Bucharest, 90-92 Sos. Panduri, 050657 Bucharest, Romania; anamaria.hanganu@unibuc.ro

⁴ National Research and Development Institute for Industrial Ecology ECOIND Bucharest, 71-73 Drumul Podul Dambovitei Street, 060652 Bucharest, Romania; gabriela.vasile@incdecoind.ro

⁵ Department of Chemistry and Chemical Engineering, Ovidius University, 124 Mamaia Blvd, 900527 Constanta, Romania

* Correspondence: gstanciu@univ-ovidius.ro (G.S.); buica_george@yahoo.com (G.-O.B.)

Received: 2 November 2020; Accepted: 26 November 2020; Published: 28 November 2020



Abstract: A new thiosemicarbazone ligand was immobilized through a Cu(I)-catalyzed click reaction on the surface of glassy carbon (GC) and electrochemically reduced graphene oxide (GC-ERGO) electrodes grafted with phenylethynyl groups. Using the accumulation at open circuit followed by anodic stripping voltammetry, the modified electrodes showed a significant selectivity and sensibility for Hg(II) ions. A detection limit of 7 nM was achieved with the GC modified electrodes. Remarkably, GC-ERGO modified electrodes showed a significantly improved detection limit (0.8 nM), sensitivity, and linear range, which we attribute to an increased number of surface binding sites and better electron transfer properties. Both GC and GC-ERGO modified electrodes proved their applicability for the analysis of real water samples.

Keywords: modified electrodes; electrochemically reduced graphene oxide; thiosemicarbazone; click chemistry; anodic stripping voltammetry; mercury determination

1. Introduction

Due to their negative impact on human health [1], the maximum permissible concentration of heavy metal ions (e.g., Pb^{2+} , Cd^{2+} , Hg^{2+} , Ni^{2+}) in environmental samples is in the part per billion (ppb) range, so their detection is a demanding issue. For example, according to European Union legislation, the maximum allowable concentration of inorganic mercury ions in drinking water is 1 ppb [2]. Both industrial activities [3,4] and climate change [5,6] can generate emissions of mercury into the environment, whether in water, soil, or air.

Various analytical techniques are currently employed for the detection of Hg(II) in environmental samples: atomic fluorescence spectrometry [7–9], UV-VIS spectrophotometry [10], inductively coupled

plasma optical emission [11,12] and mass spectrometry [13], and cold vapor generation-quartz crystal microbalance [14]. Hyphenated methods such as gas chromatography-tandem mass spectrometry [15] and high-performance liquid chromatography-inductively coupled plasma mass spectrometry [16] allow both detection and speciation of mercury compounds. Generally, these techniques require high operating costs, due to expensive equipment and sophisticated sample processing.

In this context, heavy metal analysis using electrochemical methods is becoming an alternative for more sophisticated and costly techniques [17]. Particularly suitable for the trace analysis of heavy metals is the voltammetric determination following preconcentration at electrodes modified with complexing agents, which enhances both selectivity and sensitivity [18].

A versatile method for electrode surface modification is through click reactions such as Cu(I)-catalyzed azide-alkyne cycloaddition [19], but to date there are few reports of its application for ligand-modified electrodes [20–23]. A shortcoming of this approach is that it requires substrates previously grafted with a layer containing azide or alkyne functionalities. Usually, this leads to an increase in charge transfer resistance that affects the analytical response of the modified electrode. One way to overcome this drawback is through the use of graphene substrates, which offer improved electron transfer properties [24–27].

Since it has recently been pointed out that reduced graphene oxide is beneficially utilized when the electrochemical detection mechanism is adsorptive in nature [28], as in the case of stripping voltammetry, in this work we employ glassy carbon (GC) and electrochemically reduced graphene oxide (ERGO) electrodes modified with a new thiosemicarbazone ligand for the stripping voltammetric analysis of Hg(II).

Electrode modification is accomplished using the two-step functionalization protocol recently developed in our group [29], which involves surface grafting with phenylethynyl groups via the corresponding diazonium salt and the subsequent ligand immobilization through a Cu(I)-catalyzed azide-alkyne cycloaddition. The extent of surface modification is assessed through various techniques, and we demonstrate that ERGO-based electrodes have an increased number of surface binding sites and better electron transfer properties that lead to a significant improvement in analytical performance.

2. Materials and Methods

2.1. Reagents

N,N-dimethylformamide (DMF), acetonitrile (MeCN, electronic grade, 99.999%), absolute ethanol (EtOH), diethyl ether (Et₂O), tetrabutylammonium tetrafluoroborate (TBABF₄, electrochemical grade), ferrocenemethanol (FcMeOH), bromotris(triphenylphosphine) copper(I) (CuBr(PPh₃)₃), triethylamine (TEA) and graphene oxide were purchased from Sigma-Aldrich and used as received. Acetic acid, sodium acetate and metal salts (analytical reagent grade) were purchased from Sigma-Aldrich or Merck and used without further purification.

4-(6-azidohexyl)-3-thiosemicarbazide and 4-ethynylphenyldiazonium tetrafluoroborate were synthesized as described in our previous paper [29].

All aqueous solutions were prepared using Type I ultrapure water (resistivity 18.2 MΩ·cm).

2.2. Equipment

NMR spectra were recorded on a Bruker Avance III 500 (¹H: 500 MHz, ¹³C: 125 MHz) spectrometer. Infrared spectra were recorded in the 4000–600 cm⁻¹ range, at a resolution of 4 cm⁻¹, on a Bruker Vertex 70 FT-IR spectrometer. UV-Vis spectra were recorded in the 200–850 nm range using a Jasco V-670 double-beam spectrometer fitted with a standard 1 cm quartz cuvette. Raman spectra were obtained with a Renishaw InVia confocal Raman microscope fitted with a 473 nm excitation laser, at 0.4 mW incident power and a resolution of 2 cm⁻¹. Scanning electron microscopy (SEM) investigations were carried out using a FEI Quanta Inspect F electron microscope.

X-ray photoelectron spectroscopy (XPS) analysis was performed on a Thermo Scientific K-Alpha spectrometer with a monochromated Al K α source (1486.6 eV). A combined electron/argon ion flood source was employed for charge neutralization. Survey and high-resolution spectra were recorded at pass energies of 200 eV and 20 eV, respectively. Binding energies were referenced to the C 1s peak at 284.5 eV (graphitic carbon). Atomic concentrations were calculated using sensitivity factors supplied by the instrument manufacturer.

A three-electrode electrochemical cell connected to a Metrohm Autolab PGSTAT204 potentiostat/galvanostat was used to perform the electrochemical experiments. Bare or modified glassy carbon (GC) disks (3 mm diameter, from ALS Co. Ltd. Tokyo, Japan) were used as working electrodes. A Pt wire served as counter electrode and Ag/10 mM Ag⁺, 0.1 M TBABF₄ in DMF or Ag/AgCl (3 M KCl) reference electrodes were used for nonaqueous and aqueous solutions, respectively. A Metrohm Autolab PGSTAT302N potentiostat/galvanostat fitted with a FRA32M frequency response analyzer was employed for performing electrochemical impedance spectroscopy (EIS). Impedance spectra were recorded in the 100 kHz–10 mHz frequency range, with an AC signal amplitude of 10 mV and a DC bias potential of 0.25 V.

A Thermo Scientific M6 Dual atomic absorption spectrometer (AAS) with dual background correction and a VP 100 continuous flow vapor generator (VG) was used to quantify the Hg(II) amount in tap water samples. Alternatively, a Cetac Technologies Quick Trace M-8000 Mercury Analyzer was also used for Hg(II) quantification through cold vapor atomic fluorescence spectroscopy (CV-AFS).

2.3. Procedures

2.3.1. Synthesis of Ligand L

To a solution of 0.7 g (4.7 mmol) phthalaldehydic acid in 5 mL absolute ethanol heated to reflux was added dropwise a solution of 1 g (4.7 mmol) 4-(6-azidohexyl)-3-thiosemicarbazide dissolved in 5 mL of absolute ethanol. The obtained mixture was refluxed for a period of 4 h and then cooled to room temperature. Using a rotary evaporator, about 2/3 of the ethanol was removed, and the residue was maintained at –20 °C for 24 h. The crystallized thiosemicarbazone was filtered under vacuum, and consecutively washed with cold ethanol, cold diethyl ether, and finally dried under vacuum (5 mmHg) at room temperature. Yield: 0.5 g (31%) as off-white crystals.

Characterization of ligand L:

¹H-NMR (500 MHz, DMSO-d₆, ppm) δ : 1.30–1.39 (m, 4H); 1.53–1.62 (m, 4H); 3.31 (t, J = 6.9 Hz, 2H); 3.55 (quartet, J = 6.4 Hz, 2H); 7.48 (t, J = 7.6 Hz, 1H); 7.59 (t, J = 7.3 Hz, 1H); 7.84 (d, J = 7.8 Hz, 1H); 8.24 (d, J = 7.7 Hz, 1H); 8.51 (t, J = 5.9 Hz, 1H); 8.78 (s, 1H); 11.58 (s, 1H); 13.26 (br. s, 1H).

¹³C-NMR (125 MHz, DMSO-d₆, ppm) δ : 25.84; 25.91; 28.17; 28.66; 43.37; 50.58; 127.05; 129.25; 130.04; 130.75; 131.60; 134.32; 141.00; 168.17; 177.04.

IR (ATR, cm⁻¹) $\bar{\nu}$: 3359 (ν_{NH}); 3174 (ν_{NH}); 2095 ($\nu_{\text{N=N=N}}$); 1538 ($\nu_{\text{C=N}}$)

2.3.2. Electrode Preparation

The GC electrodes coated with electrochemically reduced graphene oxide (further denoted GC-ERGO) were prepared following the procedure described in ref. [30].

The modification of GC and GC-ERGO electrodes was performed using the protocol described in our previous publication [29]. Briefly, electrodes were first grafted with phenylethynyl groups by potential cycling in a 1 mM solution of 4-ethynylphenyldiazonium tetrafluoroborate in MeCN (3 cycles between 0.3 and –0.25 V, scan rate 0.1 V s⁻¹). Next, ligand L was immobilized by immersing the electrodes for 24 h in a mixture of DMF:TEA (2.5:1 *v/v*) containing 0.5 mM L and 2 mM CuBr(PPh₃)₃. The modified electrodes (further denoted GC|click|L and GC-ERGO|click|L) were thoroughly washed with DMF and water, dried, and then kept in sealed tubes until further use.

GC disk electrodes with a diameter of 6 mm were used for SEM, XPS, and Raman spectroscopy investigations, and their modification followed the same procedure described above.

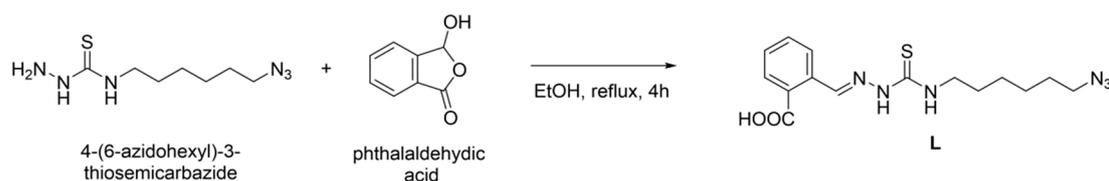
Voltammetric determinations with the modified electrodes were performed through a chemical accumulation step at open circuit followed by anodic stripping using differential pulse voltammetry (DPV) [29,31,32]. The DPV curves were recorded at 20 mV s^{-1} with an amplitude of 25 mV and 0.5 s pulse period.

The quantitation of Hg(II) in water samples was performed in an accredited laboratory, according to standardized methods: VG-AAS (calibration range $1\text{--}10 \text{ }\mu\text{g/L}$, limit of quantification $0.5 \text{ }\mu\text{g/L}$, precision 2.2% , uncertainty 11%) [33] and CV-AFS (calibration range $0.02\text{--}0.1 \text{ }\mu\text{g/L}$, limit of quantification $0.01 \text{ }\mu\text{g/L}$, precision 3.1% , uncertainty 10%) [34].

3. Results and Discussion

3.1. Preparation of Modified Electrodes

A novel thiosemicarbazone ligand (further denoted L) was synthesized by reacting 4-(6-azidoheptyl)-3-thiosemicarbazide [29] with phthalaldehydic acid (Scheme 1).



Scheme 1. Synthesis of thiosemicarbazone ligand L.

The UV-Vis spectra of ligand L recorded in the presence of 1 equivalent of different heavy metal ions (Figure 1) show a bathochromic and hypochromic shift of the absorption band at 326 nm . The most significant spectral changes occur in the presence of Hg(II) and Cu(II), which suggests that the ligand has an increased affinity for these ions. This behavior resembles that of analogous thiosemicarbazone ligands synthesized in our laboratory [29]. However, during a preliminary assessment of several azido-functionalized thiosemicarbazones, we observed a decreased sensibility of GC electrodes modified with ligand L for the voltammetric detection of Hg(II) ions. This fact prompted us to investigate an alternative electrode substrate, i.e., ERGO, in order to improve the analytical performance of the modified electrodes.

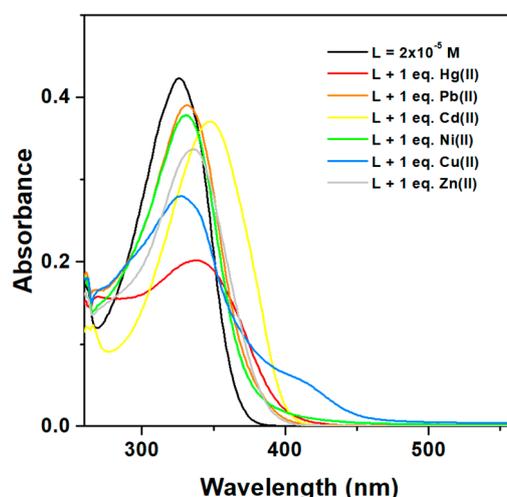


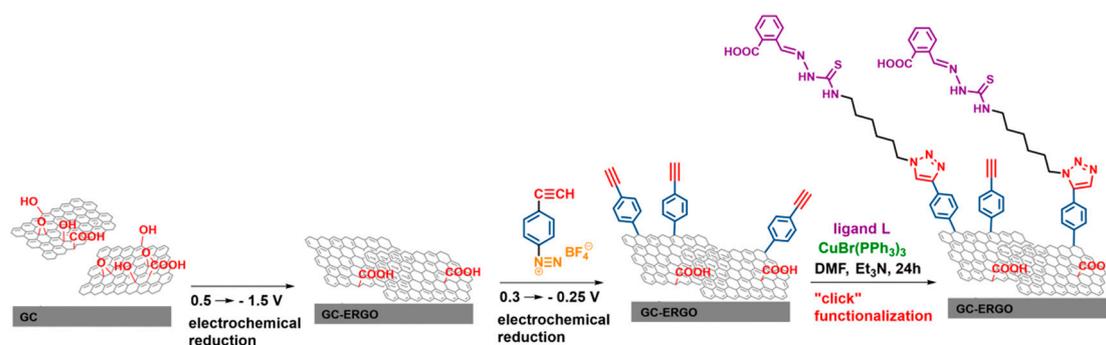
Figure 1. UV-VIS spectra of ligand L before and after the addition of 1 equivalent of heavy metal ions.

We found a single reference describing the analytical applications of a thiosemicarbazone derived from phthalaldehydic acid [35], and apparently that ligand showed a lower affinity for Hg(II) among several metal ions, in contrast to thiosemicarbazones described in our previous study [29]. This is not

surprising, since the relative stability of metal complexes depends on particular structural features of the ligand molecule. For example, it has been shown that thiosemicarbazones can act as either bidentate ligands, binding metal ions through the sulfur and the hydrazine nitrogen atoms, or tridentate species if additional coordinating groups are present (e.g., -OH groups, pyridine N) [36]. Moreover, the formation of complexes with phenyl-substituted thiosemicarbazone ligands can be influenced by noncoordinating functional groups, as the thiol-thione equilibrium is altered by electronic effects [37].

Electrochemically reduced graphene oxide (ERGO) was deposited onto glassy carbon (GC) substrates through the potentiodynamic reduction (10 cycles between 0.5 and -1.5 V, 20 mV s $^{-1}$) of a deaerated aqueous dispersion of graphene oxide (1 mg mL $^{-1}$ in pH 9.2, 0.067 M phosphate buffer) [30].

Next, the surface modification of GC and GC-ERGO electrodes was performed using the two-step protocol described in our previous paper [29] (Scheme 2). The first step consists in grafting phenylethynyl groups on the electrode surface, by cycling the potential in a solution containing the corresponding diazonium salt. The second step consists of attaching ligand L, which contains an azido group, to the alkyne-functionalized electrode through a Cu(I)-catalyzed azide-alkyne cycloaddition reaction.



Scheme 2. Preparation of GC-ERGO|click|L modified electrodes.

The cyclic voltammograms corresponding to the reduction of 4-ethynylphenyldiazonium tetrafluoroborate (1 mM in MeCN with 0.1 M TBABF $_4$) on GC and GC-ERGO electrodes are shown in Figure 2. In both cases, the first scan displays a broad and irreversible cathodic peak, but on GC-ERGO the peak current is larger (32 μ A vs. 14 μ A) and the peak potential is shifted anodically (0.02 vs. -0.11 V).

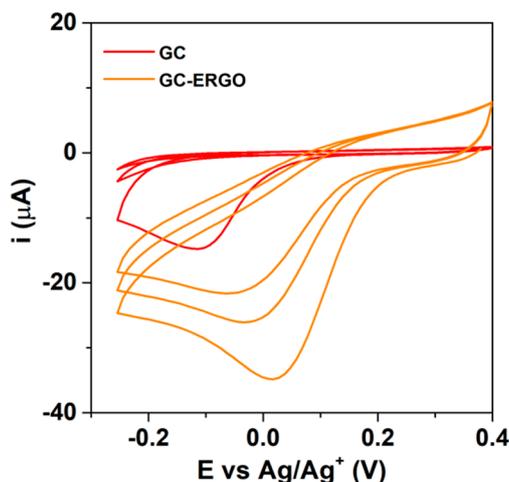


Figure 2. Cyclic voltammograms recorded in a 1 mM solution of 4-ethynylphenyldiazonium tetrafluoroborate (100 mV s $^{-1}$) at GC and GC-ERGO electrodes.

For the GC electrode, this peak disappears in the second scan since the reduction of aryldiazonium salts is self-inhibited by the grafted layers [38]. However, in the case of GC-ERGO, during the subsequent scans there is only a ~25% decrease in the peak current after each cycle, accompanied by a cathodic shift of the peak potential.

We believe the contrasting behavior of GC and GC-ERGO can be explained by considering the nature of the two electrodes, which consist of basal plane and edge plane surfaces [39]. Although reports concerning the electrochemical activity of the basal plane vs. edge plane of graphite-like materials are somewhat contradictory, recent results obtained using localized electrochemical measurements prove unequivocally that the edges and defects are more active than the basal plane, even though the latter has a non-negligible electrochemical activity [40]. This difference in reactivity was also observed in the case of the electrochemical reduction of aryldiazonium salts [38], and it was demonstrated through spatially resolved Raman spectroscopy and scanning tunneling microscopy (STM) that diazonium grafting of highly oriented pyrolytic graphite (HOPG) results in the deposition of more material at the edge planes than at the basal plane [41,42]. Moreover, in the case of graphene functionalization with diazonium salts, experimental evidence obtained using spatially and temporally resolved Raman mapping showed that nucleation sites are located on edges, and grafted regions spread from the edges toward the interior of the flakes [43,44].

It is well known that aryl radicals resulting from the electrochemical reduction of diazonium salts can react with the electrode surface or with other aryl groups already bound to the surface, leading to poly(aryl) films that grow in both two- and three-dimensions [45]. Because GC has an increased density of edge-plane sites [46], a more uniform grafting across the electrode surface leads to increased barrier properties of the aryl layers, consistent with the rapid drop in current observed in the cyclic voltammograms. Conversely, on a GC-ERGO surface dominated by lower activity basal planes, aryl radicals will react preferentially with other aryl groups and not with the surface, leading to a three-dimensional irregular growth of the layers. Presumably, such layers contain more defects (i.e., discontinuities, pores) and are less blocking, which explains the increased peak current observed in all the voltammetric cycles. There is experimental evidence that the blocking behavior of aryl multilayers does not depend on layer thickness, presumably due to their nonuniform topography [47]. At the same time, the increased amount of charge consumed during the reduction of diazonium salt at the GC-ERGO electrode suggests that in this case a higher amount of material is deposited onto the electrode surface.

3.2. Characterization of Modified Electrodes

The electrode functionalization steps were monitored through cyclic voltammetry using the ferricyanide and ferrocenemethanol redox probes [48]. Since the voltammograms (Figure 3 and Figure S3 from Supporting Information) display a quasireversible behavior of the redox couples, the peak current i_p is given by a modified version of the Randles–Ševčík equation [49]:

$$i_p = (2.69 \times 10^5) n^{3/2} A D^{1/2} C v^{1/2} K(\Lambda, \alpha) \quad (1)$$

where n is the number of transferred electrons, A the electrode area (cm^2), D the diffusion coefficient of the redox probe ($\text{cm}^2 \text{s}^{-1}$), C the bulk concentration of the redox probe (mol cm^{-3}), v the scan rate (V s^{-1}) and $K(\Lambda, \alpha)$ is a function that depends on the rate parameter Λ and the charge transfer coefficient α [50]. The rate parameter Λ is defined as:

$$\Lambda = \pi^{1/2} \Psi = k^\circ (D_O^{1-\alpha} D_R^\alpha n f v)^{-1/2} \quad (2)$$

where Ψ is a dimensionless charge transfer parameter [51], k° is the standard heterogeneous rate constant (cm s^{-1}), D_O the diffusion coefficient of the oxidized species, D_R the diffusion coefficient of the reduced species, and $f = F/RT$ with F , R and T having their usual meaning.

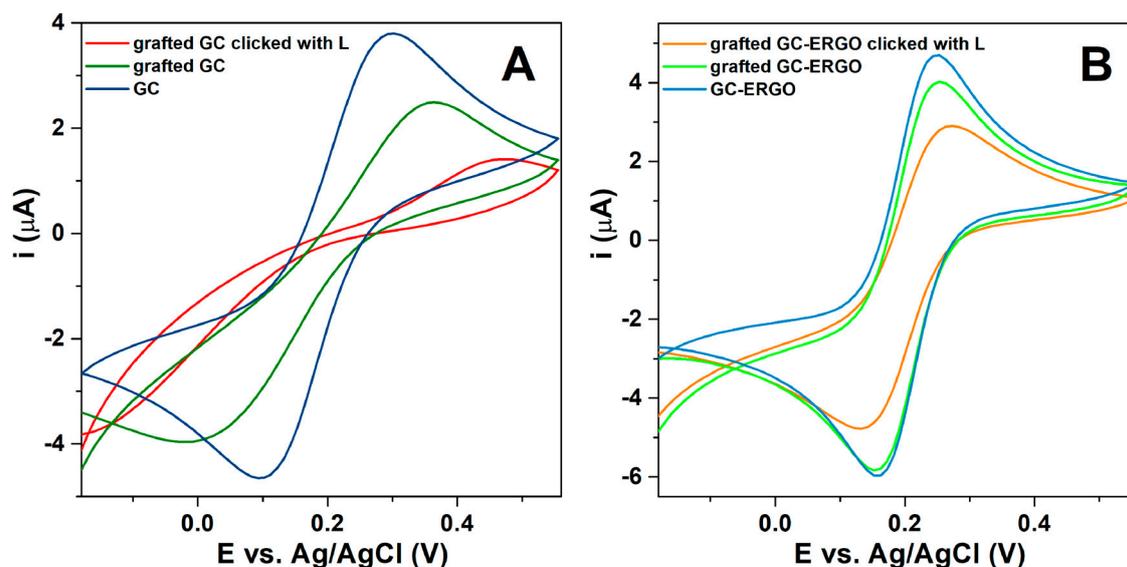


Figure 3. Cyclic voltammograms recorded in 1 mM $\text{Fe}(\text{CN})_6^{3-}$, 0.1 M KCl solution (20 mV s^{-1}), at (A) GC and (B) GC-ERGO electrodes, after different modification steps.

The parameters ψ and $K(\Lambda, \alpha)$ were estimated using the equations given in ref. [52] and Figure 4 from ref. [50], respectively. The values of the diffusion and transfer coefficients were taken from the literature: for $\text{Fe}(\text{CN})_6^{3-}$, $\alpha = 0.5$, $D_{\text{O}} = 7.6 \times 10^{-6} \text{ cm}^2 \text{ s}^{-1}$, $D_{\text{R}} = 6.5 \times 10^{-6}$ and for FcMeOH $\alpha = 0.5$ and $D_{\text{O}} = D_{\text{R}} = 7.8 \times 10^{-6} \text{ cm}^2 \text{ s}^{-1}$ [53,54].

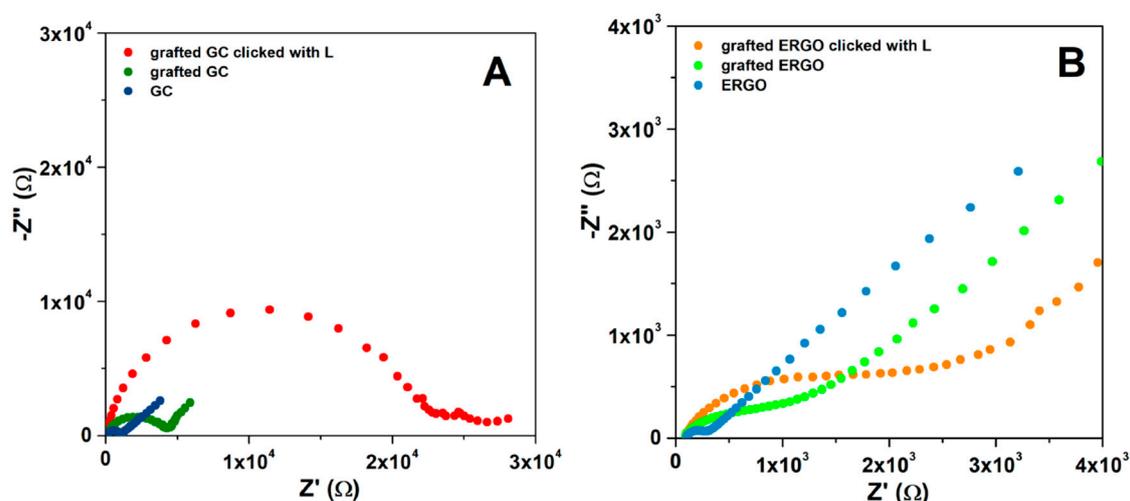


Figure 4. Electrochemical impedance spectra (Nyquist plots) recorded in 5 mM $\text{Fe}(\text{CN})_6^{3-/4-}$, 0.1 M KCl solution, at (A) GC and (B) GC-ERGO electrodes, at different modification steps.

There are no major differences in the electrochemical response of the $\text{FcMeOH}^{0/+}$ on the unmodified GC and GC-ERGO electrodes (Figure S3 from Supporting Information), so this redox probe was employed mainly for determining electroactive surface areas, which are $6.9 \times 10^{-2} \text{ cm}^2$ for GC and $9.9 \times 10^{-2} \text{ cm}^2$ for the ERGO electrode substrate, respectively. It should be noted that experimental evidence presented in the following sections suggests that the 43% increase in surface area determined for GC-ERGO is not solely responsible for the contrasting behavior of the two modified electrodes.

Because the $\text{Fe}(\text{CN})_6^{3-}$ electron transfer kinetics is very sensitive to surface chemistry [55], it is more suitable to monitor electrode modification. As expected, the heterogeneous electron transfer rate constant (k° , Table 1) decreases by a factor of ~ 3 following the GC electrode modification

with phenylethynyl groups. Interestingly, k° decreases almost 15 times after performing the click functionalization step.

Table 1. Electrochemical parameters determined from cyclic voltammograms recorded in 0.5 mM FcMeOH, 0.1 M KCl and 1 mM $\text{Fe}(\text{CN})_6^{3-}$, 0.1 M KCl solutions, at GC and GC-ERGO electrodes, after various modification steps.

Electrode	Redox Probe	$E_{p,a}$ (V)	$E_{p,c}$ (V)	ΔE_p (V)	$i_{p,a}$ (A)	$i_{p,c}$ (A)	ψ	$K(\Lambda, \alpha)$	k° (cm s^{-1})
GC	FcMeOH	0.20	0.12	0.08	3.4×10^{-6}	3.4×10^{-6}	1.3	0.96	5.6×10^{-3}
GC-ERGO		0.21	0.14	0.07	5.2×10^{-6}	5.2×10^{-6}	2.5	0.98	1.1×10^{-2}
GC	$\text{Fe}(\text{CN})_6^{3-}$	0.30	0.10	0.20	5.4×10^{-6}	5.5×10^{-6}	0.087	-	3.6×10^{-4}
GC grafted ^{a)}		0.36	0.02	0.34	3.7×10^{-6}	4.1×10^{-6}	0.031	-	1.3×10^{-4}
GC click L		0.46	-0.17	0.63	-	-	0.002	-	8.3×10^{-6}
GC-ERGO		0.24	0.15	0.09	6.8×10^{-6}	6.8×10^{-6}	0.83	-	3.4×10^{-3}
GC-ERGO grafted ^{a)}		0.25	0.15	0.10	6.3×10^{-6}	6.3×10^{-6}	0.59	-	2.4×10^{-3}
GC-ERGO click L		0.27	0.13	0.14	5.1×10^{-6}	5.2×10^{-6}	0.24	-	9.9×10^{-4}

^{a)} electrode grafted with phenylethynyl groups.

On the contrary, when using GC-ERGO electrodes as substrates, the $\text{Fe}(\text{CN})_6^{3-}$ electron transfer kinetics does not show significant changes (Figure 3B), as k° decreases only ~ 1.5 times after grafting and again ~ 2.5 times after performing the click reaction. This indicates that a modified GC-ERGO surface is significantly less blocked (k° is two orders of magnitude higher), which is entirely consistent with the behavior during grafting with diazonium salt.

Electrochemical impedance spectroscopy (EIS) in the presence of $\text{Fe}(\text{CN})_6^{3-/4-}$ as redox probe was further used to evaluate the surface modification of GC and GC-ERGO electrodes. The corresponding Nyquist plots are shown in Figure 4, and charge-transfer resistance (R_{CT}) values were obtained by fitting the data with a Randles equivalent circuit [56]. The charge-transfer resistance increases from ~ 0.9 k Ω to ~ 3.8 k Ω after grafting the GC electrode with phenylethynyl groups. Again, a significant blocking can be observed following the click functionalization step, as R_{CT} increases to ~ 22.5 k Ω . In the case of GC-ERGO electrode, R_{CT} increases after grafting from 0.18 k Ω to 1.18 k Ω , and after the second step to 2.24 k Ω . It should be noted that the R_{CT} value for the GC-ERGO modified electrode is lower by one order of magnitude than the GC modified electrode, in agreement with the CV results.

Next, the surface of the modified GC and GC-ERGO electrodes was investigated using XPS, and the corresponding survey spectra are shown in Figure 5. The C/N atomic ratios presented in Table 2 seem to indicate a higher degree of functionalization for GC-ERGO|click|L (C/N = 37.2) than GC|click|L (C/N = 64.2), which correlates with the increased amount of charge consumed during grafting with diazonium salt. Moreover, when the two electrodes were immersed in a solution containing 10^{-6} M Hg(II) for 1 h, washed and then analyzed using XPS, the C/Hg ratio is ~ 2 times lower for GC-ERGO|click|L than GC|click|L although the N/Hg ratio is the same for both electrodes. Undoubtedly a higher degree of surface modification with phenylethynyl groups led to an increased concentration of surface-bound ligand L.

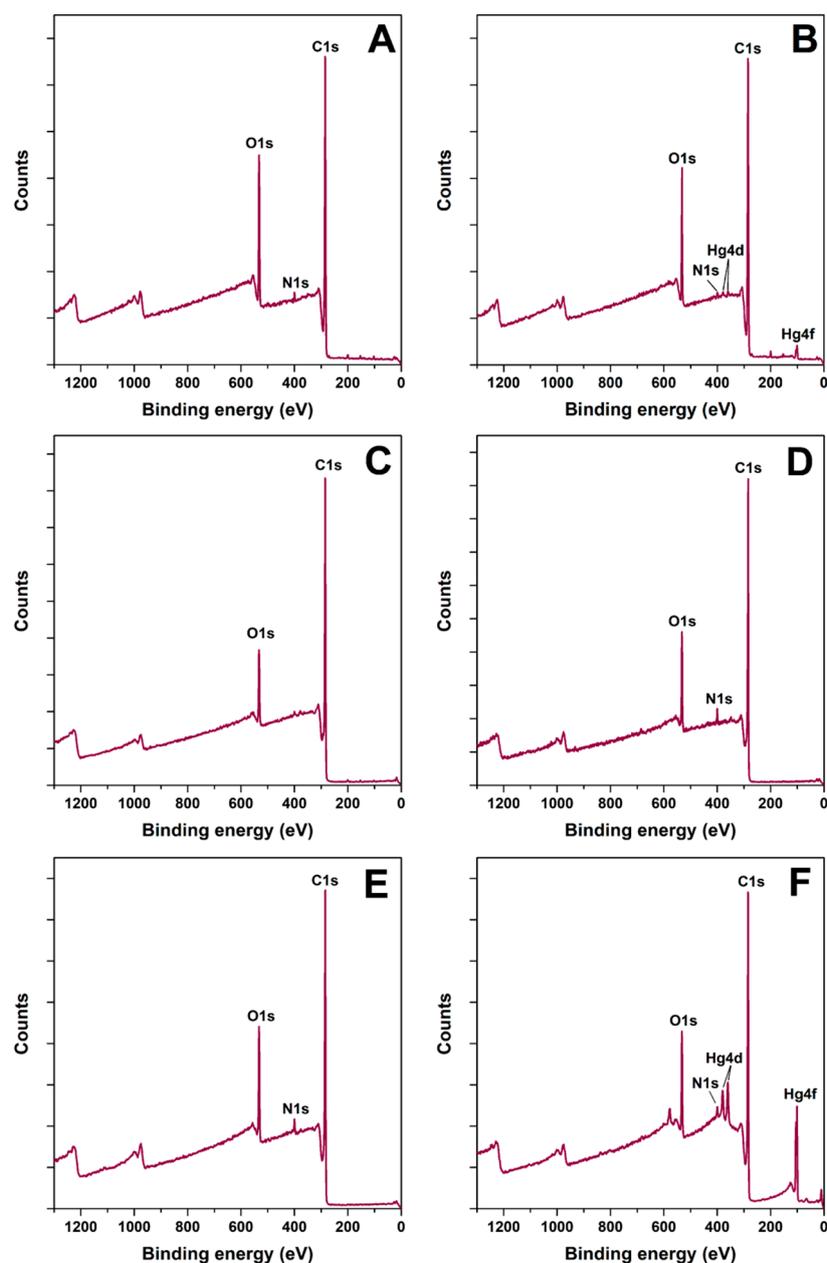


Figure 5. XPS survey spectra of GC and GC-ERGO electrodes after various modification steps: (A) GC|click|L; (B) GC|click|L treated in a Hg(II) solution; (C) GC-ERGO; (D) GC-ERGO grafted with phenylethynyl groups; (E) GC-ERGO|click|L; (F) GC-ERGO|click|L treated in a Hg(II) solution.

Table 2. Atomic composition of the electrode surface after various modification steps.

Electrode	Atomic Concentration (%)				Atomic Ratios			
	C 1s	O 1s	N 1s	Hg 4f	C/O	C/N	C/Hg	N/Hg
GC click L	83.0	15.9	1.1	-	5.6	64.2	-	-
GC click L + Hg(II) ^{a)}	82.9	15.3	1.1	0.7	5.6	60.8	106.9	1.2
GC-ERGO	90.6	8.2	1.2	-	10.4	68.3	-	-
GC-ERGO grafted ^{b)}	86.9	11.0	2.1	-	7.3	34.0	-	-
GC-ERGO click L	85.2	12.3	2.5	-	6.8	37.2	-	-
GC-ERGO click L + Hg(II) ^{a)}	85.1	11.6	2.0	1.3	7.1	34.5	42.6	1.2

^{a)} electrode treated in a solution containing Hg(II) ions and then washed; ^{b)} GC-ERGO electrode grafted with phenylethynyl groups.

The electrode surface modification was also assessed using Raman spectroscopy. The Raman spectra (Figure S4 from Supporting Information) display the G band ($\sim 1580\text{ cm}^{-1}$) characteristic for the sp^2 -hybridized carbon lattice and the defect-related D band ($\sim 1360\text{ cm}^{-1}$), the intensity ratio I_D/I_G being related to the number of sp^3 defect sites [57]. After functionalization both the GC and GC-ERGO electrodes show an increase in the I_D/I_G ratio, from 1.31 to 1.41 in the former case and from 1.02 to 1.26 in the latter case, which confirms the covalent attachment of aryl radicals generated through the electrochemical reduction of diazonium salt. Because the differences between the I_D/I_G ratios before and after modification are quite similar, and taking into account the greater amount of grafting in the case of GC-ERGO|click|L, supports the idea of a three-dimensional layer growth in the case of graphene.

The surface morphology of unmodified and modified GC-ERGO electrodes was further examined using SEM (Figure S5A,B from Supporting Information). The micrographs reveal an incomplete coverage of the GC substrate with agglomerates consisting of stacked ERGO sheets, in line with previous observations [58]. Moreover, there seems to be no apparent difference between the electrode surface morphology before and after modification. Interestingly, the micrograph of an GC-ERGO|click|L electrode treated in a 10^{-6} M Hg(II) solution and imaged using backscattered electrons (Figure S5C) suggests that ERGO agglomerates, which appear lighter, contain an increased amount of mercury.

3.3. Voltammetric Detection of Hg(II)

Furthermore, the complexation of several heavy metal ions in heterogenous phase was investigated using GC|click|L modified electrodes. Figure 6 shows the response of the modified electrode after 10 min accumulation at open circuit in acetate buffer (pH 4.5). The GC|click|L electrode shows a DPV response only for mercury ions, which appear as a stripping peak at $\sim 0.24\text{ V}$. Considering the selectivity for Hg(II), which seems to be characteristic for electrodes modified with thiosemicarbazone ligands when the complexation is performed at open circuit [29], the performances of GC|click|L were further evaluated only for this ion.

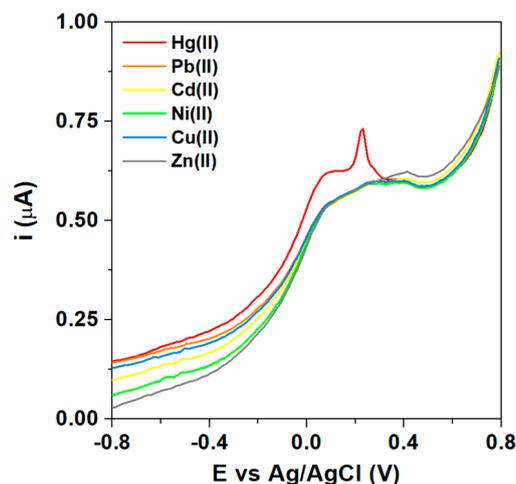


Figure 6. Differential pulse voltammetry (DPV) curves recorded on a GC|click|L modified electrode after 10 min accumulation in acetate buffer (pH 4.5) containing $5 \times 10^{-8}\text{ M}$ of various heavy metal ions.

Next, in order to investigate the effect of electrode preparation conditions on the Hg(II) response, DPV curves were recorded in a $5 \times 10^{-8}\text{ M}$ Hg(II) solution on several GC|click|L modified electrodes prepared using a different number of potential cycles during grafting with diazonium salt (Figure 7). After an initial increase up to three potential cycles, the stripping current starts to drop. This observation implies that two opposite effects influence the electrode response: the amount of surface-bound ligand L increases with the number of potential cycles employed for grafting, leading to an enhanced stripping current, but at the same time the layers become more blocking and the stripping current decreases when the grafted layer becomes too thick. It should be noted at this point that, in order to allow for

a meaningful comparison, identical functionalization conditions were employed for both GC and GC-ERGO substrates, although in the latter case the improved electron transfer properties of the grafted layer suggest that the analytical performance can be further enhanced by increasing the amount of surface-bound ligand.

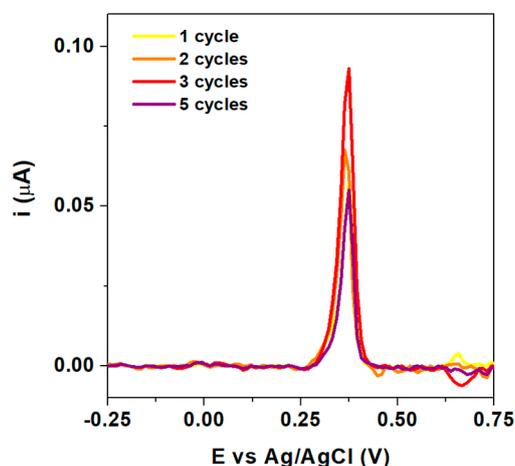


Figure 7. DPV curves (background corrected) recorded in a solution containing 5×10^{-8} M Hg(II) on GC|click|L modified electrodes prepared using different number of scans during grafting with diazonium salt.

The analytical response GC|click|L modified electrodes towards Hg(II) was further optimized considering several analytical parameters. Because the pH has a major influence on the formation of complexes with thiosemicarbazone ligands [36] and at the same time determines the mercury speciation [59], we investigated the GC|click|L electrode response in the pH range 3 to 6 (Figure S6A from Supporting Information). Since the best response was attained at pH 4, this value was maintained for the analytical determinations. Above this pH value, the Hg(II) peak current decreases slightly, probably as a consequence of hydrolysis reactions which lead to basic salts [60]. This is in agreement with previous observations [29,61]. Furthermore, a steady increase of the stripping current was observed for accumulation times up to 10 min (Figure S6B from Supporting Information), suggesting that at this point most surface sites become occupied by Hg(II) ions. To achieve the best sensitivity, an accumulation time of 15 min was chosen for analytical determinations. Finally, we investigated the influence of the reduction potential and reduction time on the stripping current, and we found that a potential of -0.9 V and a time of 180 s allowed the complete reduction of accumulated mercury ions (Figure S6C,D from Supporting Information).

The analytical performance of the modified electrodes was further assessed using the optimized DPV method (Figure 8 and Table 3). The GC|click|L electrodes exhibit a narrow linear dependence between the stripping peak current and Hg(II) concentration (Figure 8B) and a relatively good limit of detection (LOD, estimated as 3-times signal-to-noise ratio). However, when the same analyses were performed with GC-ERGO|click|L electrodes (Figure 8C), the analytical performance was substantially improved (Table 3). These electrodes showed a wider linear range, a LOD which is ten times lower and a two-fold increase in sensitivity (Figure 8D).

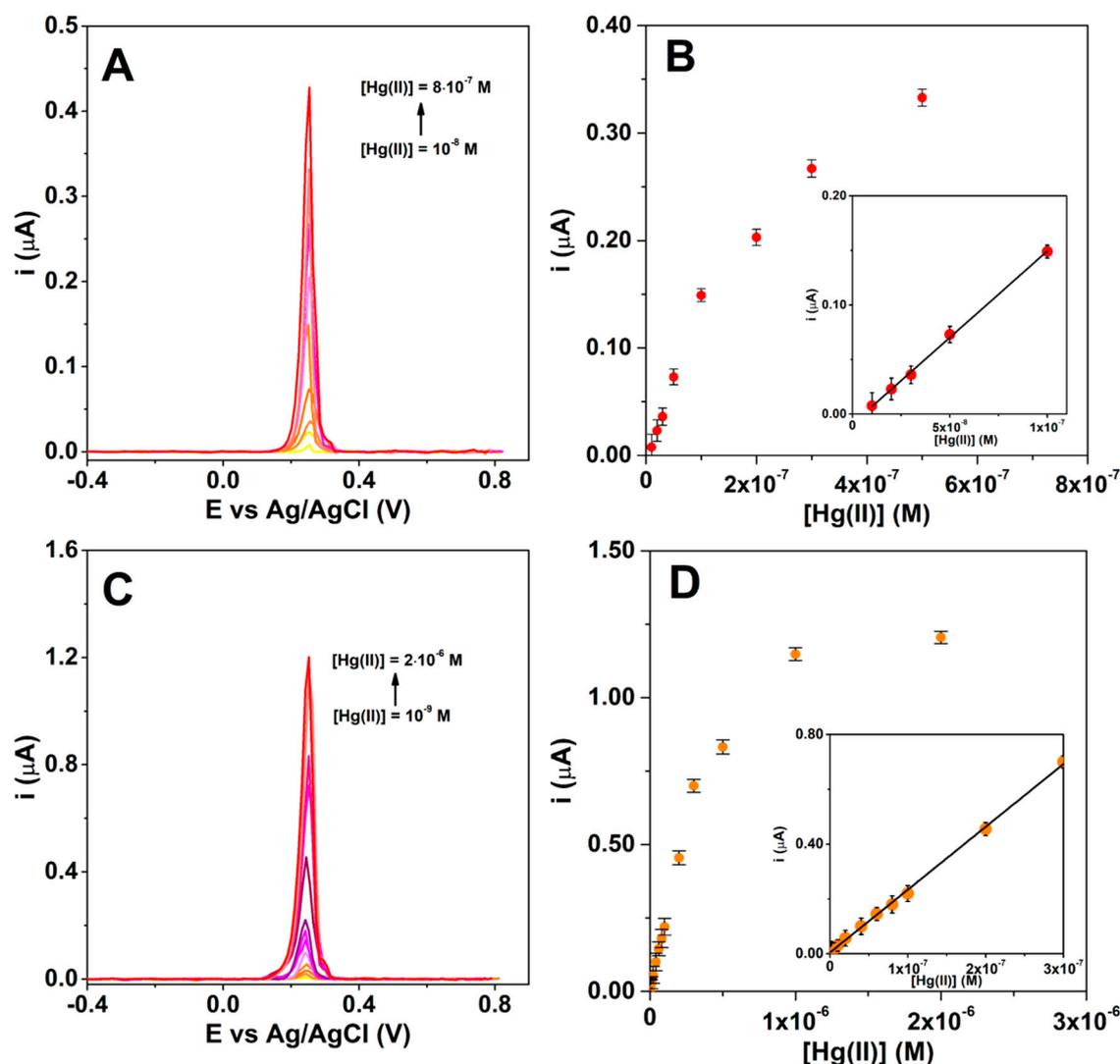


Figure 8. Typical DPV curves (A,C) and calibration plots (B,D) for Hg(II) analysis with GC|click|L (A,B) and GC-ERGO|click|L (C,D) modified electrodes. All DPV curves are background corrected.

Table 3. Analytical performance of GC|click|L and GC-ERGO|click|L modified electrodes for Hg(II) sensing.

Electrode	Linearity Domain (M)	Linear Regression Equation	Limit of Detection (M)
GC click L	$10^{-8} \div 10^{-7}$	$i \text{ (A)} = 8 \times 10^{-9} + 1.58C \text{ (M)}; R^2 = 0.998$	7×10^{-9}
GC-ERGO click L	$10^{-9} \div 3 \times 10^{-7}$	$i \text{ (A)} = 4.5 \times 10^{-9} + 2.3C \text{ (M)}; R^2 = 0.9996$	8×10^{-10}

We believe the improved linearity at the lower range of Hg(II) concentrations and lower LOD obtained with GC-ERGO electrodes are consistent with an increased amount of surface-bound ligand, which facilitates Hg(II) adsorption, leading in turn to enhanced stripping currents. This would be in agreement with the CV, XPS, SEM, and Raman spectroscopy results discussed in the previous sections. Moreover, this might also explain the improved linearity at higher analyte concentrations, as it is well known that deviations from linearity appear when surface sites become saturated [62].

3.4. Reproducibility, Interference, and Real Sample Analysis

The reproducibility concerns both electrode preparation and the possibility of reusing the same electrode for repeated Hg(II) determinations. Consequently, five GC and five GC-ERGO electrodes were functionalized with L and employed for the analysis of a solution containing 8×10^{-8} M Hg(II). Relative

standard deviations (RSD) of 3.56% and 4.26% were obtained for the GC|click|L and GC-ERGO|click|L electrodes, respectively, which indicate a good reproducibility of the electrode preparation procedure.

Undoubtedly, the possibility of using the same electrode for multiple determinations is also an important factor when considering a new electroanalytical method. As previously reported for electrodes modified with thiosemicarbazone ligands [29], an effective regeneration of GC|click|L and GC-ERGO|click|L electrodes was achieved by competitive chemical decomplexation in a solution of sodium diethyldithiocarbamate (Figure S7 from Supporting Information). For the GC|click|L electrode, RSDs of 4.13% and 12.9% were obtained after 5 and 10 consecutive Hg(II) determinations. Rather similar values were observed for the GC-ERGO|click|L electrode, where RSDs of 4.92% and 13.6% were attained after 5 and 10 measurements, respectively. This indicates that both modified electrodes can be used for up to 5 Hg(II) determinations, after which the regeneration treatment starts to affect the electrode surface.

Next, the interfering effect of heavy metal ions usually found in water (a mixture of Zn^{2+} , Cd^{2+} , Pb^{2+} , Ni^{2+} , and Cu^{2+} , further denoted *Int*) on the analysis of solutions containing 8×10^{-8} M Hg^{2+} was investigated. As can be seen in Figure 9, the Hg(II) stripping current deviates less than $\pm 5\%$ up to an excess of five equivalents of *Int*. At higher concentrations of *Int*, the stripping current decreases and a new peak appears at -0.6 V, which we attribute to the redissolution of Pb(II) ions retained on the electrode surface. This indicates that a part of the surface sites become occupied by Pb(II) ions, leading to a decrease in the amount of Hg(II) ions accumulated on the electrode surface.

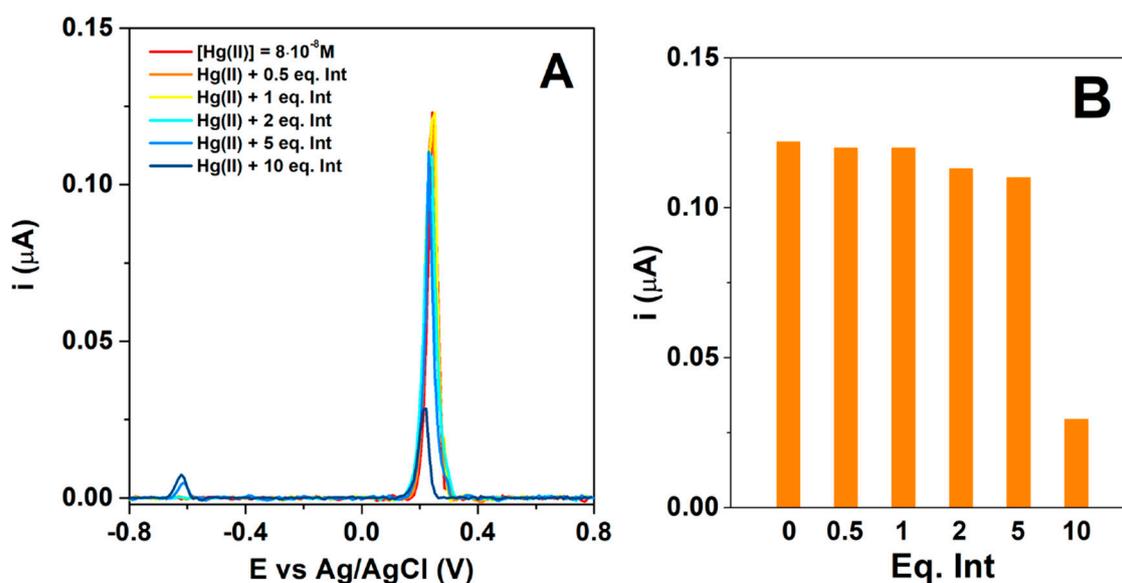


Figure 9. DPV curves (background corrected) recorded on a GC|click|L modified electrode (A) and Hg(II) stripping current intensity (B) in the presence of a mixture of interfering ions.

Lastly, the detection of mercury ions from tap water samples was performed using the modified electrodes, and results were compared with values obtained using standard AAS and AFS methods (Table 4). The good correlation between these methods, with a recovery between 97% and 103%, proves that both GC|click|L and GC-ERGO|click|L electrodes can be employed successfully for the anodic stripping voltammetric determination of mercury ions in real water samples.

The uncertainty budget for the voltammetric determinations was evaluated taking into account both electrode preparation and the voltammetric determination procedures. The obtained uncertainty values are 18.6% and 21.0% for the GC|click|L and GC-ERGO|click|L electrodes, respectively. Furthermore, the RSD of the voltammetric determinations falls below the limits recommended in the literature, i.e., a maximum RSD of 45.3% for 1 $\mu g/L$ and 32% for 10 $\mu g/L$ [63]. Finally, the recovery

percentages for all the analyzed samples fall in the recommended range, which is between 40% and 120% for 1 µg/L, and between 60% and 115% for 10 µg/L [63].

Table 4. Determination of Hg(II) in tap water using GC|click|L and GC-ERGO|click|L modified electrodes. For comparison, Hg(II) concentrations were also determined using standard AAS and AFS methods.

Sample	Added Hg(II) (M)	Method			
		GC Click L	GC-ERGO Click L	VG-AAS	CV-AFS
Tap water	-	ND ^a	ND	ND	ND
Spiked tap water I	2.5×10^{-8}	$2.47 (\pm 0.46) \times 10^{-8}$	$2.48 (\pm 0.52) \times 10^{-8}$	$2.61 (\pm 0.31) \times 10^{-8}$	$2.54 (\pm 0.25) \times 10^{-8}$
Spiked tap water II	1×10^{-7}	$0.97 (\pm 0.18) \times 10^{-7}$	$0.95 (\pm 0.20) \times 10^{-7}$	$0.93 (\pm 0.11) \times 10^{-7}$	$1.02 (\pm 0.10) \times 10^{-7}$

^a Not detected.

4. Conclusions

Glassy carbon (GC) and electrochemically reduced graphene oxide (ERGO) electrodes modified with a new thiosemicarbazone ligand were prepared using a two-step functionalization protocol which involves surface grafting with phenylethynyl groups via the corresponding diazonium salt and the subsequent ligand immobilization through an azide-alkyne cycloaddition catalyzed by Cu(I). The extent of surface modification was assessed through various techniques, and we demonstrate that in the case of ERGO, the diminished self-inhibition of diazonium reduction allows a higher degree of surface functionalization and leads to improved electron transfer properties of the grafted layers.

Using the accumulation at open circuit followed by anodic stripping voltammetry for the determination of Hg(II) ions, we demonstrate that ERGO outperforms GC as a substrate for obtaining ligand-modified electrodes, at least when the modification strategy is based on aryldiazonium chemistry. In the case of ERGO, the increased number of surface binding sites extends the linearity domain in both lower and upper analyte concentration ranges, and, at the same time, the reduced blocking effect of the grafted layers is probably responsible for the improved sensitivity of these electrodes.

Supplementary Materials: The following are available online at <http://www.mdpi.com/1424-8220/20/23/6799/s1>, Figure S1: ¹H-NMR (500 MHz) and ¹³C-NMR (125 MHz) spectra of thiosemicarbazone ligand L (DMSO-d₆), Figure S2: Infrared spectrum of thiosemicarbazone ligand L, Figure S3: Cyclic voltammograms recorded in 1 mM ferrocenemethanol, 0.1 M KCl solution (20 mV s⁻¹), on (A) GC and (B) GC-ERGO electrodes, Figure S4: Raman spectra of (A) GC, (B) GC|click|L, (C) GC-ERGO and (D) GC-ERGO|click|L electrodes, Figure S5: SEM micrographs of the electrode surfaces for A) GC-ERGO, B) GC-ERGO|click|L, C) GC-ERGO|click|L treated in a Hg(II) solution (backscattered electron detector), Figure S6: The effect of (A) pH of the accumulation solution, (B) accumulation time at open circuit, (C) deposition potential and (D) time for the reduction of accumulated ions, on the Hg(II) stripping current recorded with a GC|click|L modified electrode, Figure S7: Hg(II) DPV curves recorded on GC|click|L electrodes before and after decomplexation in 1 mM sodium diethyldithiocarbamate solution.

Author Contributions: G.-O.B. and M.D.R. designed the study, methodology, supervision and wrote the main manuscript text. M.D.R. performed the synthesis and oversaw the characterization of 4-phenylethynyl diazonium tetrafluoroborate and thiosemicarbazone ligand. I.G.B. and G.S. performed the electrochemical experiments and wrote the corresponding part of the manuscript. A.M.P. and C.D. performed the XPS and Raman characterization and wrote the corresponding part of the manuscript. E.V. and C.P. performed the SEM investigations and wrote the corresponding part of the manuscript. A.H. carried out the characterization of 4-phenylethynyl diazonium tetrafluoroborate and thiosemicarbazone ligand. I.G.B. and G.-G.V. performed the analytical determinations. G.-G.V. performed the atomic spectrometry experiments. All authors have read and agreed to the published version of the manuscript.

Funding: This research was funded by Romanian National Authority for Scientific Research, UEFISCDI, under grant PN-III-P1-1.1-TE-2016-0860, contract no. 114/2018.

Acknowledgments: Ioana Georgiana Bugean thanks to Operational Programme Human Capital of the Ministry of European Funds through the Financial Agreement 51668/09.07.2019, SMIS code 124705. The University of Bucharest NMR facility equipment is supported financially through grants European Regional Development Fund through Competitiveness Operational Program 2014-2020, Priority axis 1, Project No. P_36_611, MySMIS code 107066 and UniRem no. 244 and FDI-2020-0355.

Conflicts of Interest: The authors declare no conflict of interest.

References

1. Fu, Z.; Xi, S. The effects of heavy metals on human metabolism. *Toxicol. Mech. Methods* **2020**, *30*, 167–176. [[CrossRef](#)] [[PubMed](#)]
2. Council Directive 98/83/EC of 3 November 1998 on the Quality of Water Intended for Human Consumption. Available online: <http://data.europa.eu/eli/dir/1998/83/oj> (accessed on 27 October 2015).
3. Saleh, T.A.; Fadillah, G.; Ciptawati, E.; Khaled, M. Analytical methods for mercury speciation, detection, and measurement in water, oil, and gas. *Trends Anal. Chem.* **2020**, *132*, 116016. [[CrossRef](#)]
4. Vasile, G.G.; Gheorghe, S.; Ene, C.; Serban, E.A.; Stoica, C. Total mercury in fish and benthic invertebrates collected from Olt River, Romania. *Rev. Chim.* **2019**, *70*, 263–268. [[CrossRef](#)]
5. Wijngaard, R.R.; van der Perk, M.; van der Grift, B.; de Nijs, T.C.M.; Bierkens, M.F.P. The Impact of Climate Change on Metal Transport in a Lowland Catchment. *Water Air Soil Pollut.* **2017**, *228*, 107. [[CrossRef](#)] [[PubMed](#)]
6. Shrestha, S.; Gunawardana, S.K.; Piman, T.; Babel, M.S. Assessment of the impact of climate change and mining activities on streamflow and selected metal's loading in the Chindwin River, Myanmar. *Environ. Res.* **2020**, *181*, 108942. [[CrossRef](#)] [[PubMed](#)]
7. Vasile, G.G.; Marin, N.M.; Cruceru, L.V.; Simion, M.; Galaon, T.; Lehr, C.B. Determination of ultra-trace mercury in water samples based on cold vapor atomic fluorescence spectrometry using a gold trap. *Rev. Chim.* **2016**, *67*, 1427–1432.
8. Hu, P.Y.; Wang, X.; Yang, L.; Yang, H.Y.; Tang, Y.Y.; Luo, H.; Xiong, X.L.; Jiang, X.; Huang, K. Speciation of mercury by hydride generation ultraviolet atomization-atomic fluorescence spectrometry without chromatographic separation. *Microchem. J.* **2018**, *143*, 228–233. [[CrossRef](#)]
9. Tassone, A.; Moretti, S.; Martino, M.; Pirrone, N.; Sprovieri, F.; Naccarato, A. Modification of the EPA method 1631E for the quantification of total mercury in natural waters. *Methods X* **2020**, *7*, 100987. [[CrossRef](#)]
10. Janani, B.; Syed, A.; Raju, L.; Marraiki, N.; Elgorban, A.M.; Zaghloul, S.S.; Thomas, A.M.; Das, A.; Sudheer, K.S. Highly selective and effective environmental mercuric ion detection method based on starch modified Ag NPs in presence of glycine. *Opt. Commun.* **2020**, *465*, 125564. [[CrossRef](#)]
11. Fernández, Z.H.; Rojas, L.A.V.; Álvarez, A.M.; Álvarez, J.R.E.; dos Santos Júnior, J.A.; González, I.P.; González, M.R.; Macias, N.A.; Sánchez, D.L.; Torres, D.H. Application of Cold Vapor-Atomic Absorption (CVAAS) Spectrophotometry and Inductively Coupled Plasma-Atomic Emission Spectrometry methods for cadmium, mercury and lead analyses of fish samples. Validation of the method of CVAAS. *Food Control* **2015**, *48*, 37–42. [[CrossRef](#)]
12. Angyus, S.B.; Darvasi, E.; Ponta, M.; Petreus, D.; Eitz, R.; Senila, M.; Frentiu, M.; Frentiu, T. Interference-free, green microanalytical method for total mercury and methylmercury determination in biological and environmental samples using small-sized electrothermal vaporization capacitively coupled plasma microtorch optical emission spectrometry. *Talanta* **2020**, *217*, 121067. [[CrossRef](#)] [[PubMed](#)]
13. Mohibul Kabir, K.M.; Jampaiah, D.; Kandjani, A.E.; Mullett, M.; Tardio, J.; Sabri, Y.M.; Bhargava, S.K. Cold vapor integrated quartz crystal microbalance (CV-QCM) based detection of mercury ions with gold nanostructures. *Sensor. Actuator. B Chem.* **2019**, *290*, 453–458. [[CrossRef](#)]
14. Samaz, M.; Akgul, B.; Yildirim, D.; Sazmaz, A. Mercury uptake and phytotoxicity in terrestrial plants grown naturally in the Gumuskoy (Kutahya) mining area, Turkey. *Int. J. Phytoremediat.* **2016**, *18*, 69–76. [[CrossRef](#)] [[PubMed](#)]
15. Li, J.; He, Q.; Wu, L.; Sun, J.; Zheng, F.; Li, L.; Liu, W.; Liu, J. Ultrasensitive speciation analysis of mercury in waters by headspace solid-phase microextraction coupled with gas chromatography-triple quadrupole mass spectrometry. *Microchem. J.* **2020**, *153*, 104459. [[CrossRef](#)]
16. Jia, X.; Zhao, J.; Ren, H.; Wang, J.; Hong, Z.; Zhang, X. Zwitterion-functionalized polymer microspheres-based solid phase extraction method on-line combined with HPLC-ICP-MS for mercury speciation. *Talanta* **2019**, *196*, 592–599. [[CrossRef](#)] [[PubMed](#)]
17. Ferrari, A.G.-M.; Carrington, P.; Rowley-Neale, S.J.; Banks, C.E. Recent advances in portable heavy metal electrochemical sensing platforms. *Environ. Sci. Water Res. Technol.* **2020**, *6*, 2676–2690. [[CrossRef](#)]
18. Gao, C.; Huang, X.-J. Voltammetric determination of mercury(II). *Trends Analyt. Chem.* **2013**, *51*, 1–12.

19. Yáñez-Sedeño, P.; González-Cortés, A.; Campuzano, S.; Pingarrón, J.M. Copper(I)-Catalyzed Click Chemistry as a Tool for the Functionalization of Nanomaterials and the Preparation of Electrochemical (Bio)Sensors. *Sensors* **2019**, *19*, 2379. [CrossRef]
20. Qiu, S.; Xie, L.; Gao, S.; Liu, Q.; Lin, Z.; Qiu, B.; Chena, G. Determination of copper(II) in the dairy product by an electrochemical sensor based on click chemistry. *Anal. Chim. Acta* **2011**, *707*, 57–61. [CrossRef]
21. Tang, Y.; Zhang, J.; Tang, D.; Teng, L.; Lv, J.; Tang, D. Click-conjugation of nanogoldfunctionalized PAMAM dendrimer: Toward a novel electrochemical detection platform. *Electroanalysis* **2015**, *27*, 2280–2285. [CrossRef]
22. Tang, D.; Zhang, J.; Tang, Y.; Teng, L.; Xia, B.; Tang, D. Hairpin DNA-dependent click conjugation of oligonucleotides for electrochemical monitoring of copper(II). *Electroanalysis* **2015**, *27*, 2513–2517. [CrossRef]
23. Fomo, G.; Nwaji, N.; Nyokong, T. Low symmetric metallophthalocyanine modified electrode via click chemistry for simultaneous detection of heavy metals. *J. Electroanal. Chem.* **2018**, *813*, 58–66. [CrossRef]
24. Ambrosi, A.; Chua, C.K.; Bonanni, A.; Pumera, M. Electrochemistry of Graphene and Related Materials. *Chem. Rev.* **2014**, *114*, 7150–7188. [CrossRef] [PubMed]
25. Nag, A.; Mitra, A.; Mukhopadhyay, S.C. Graphene and its sensor-based applications: A review. *Sens. Act. A Physical* **2018**, *270*, 177–194. [CrossRef]
26. Sang, M.; Shin, J.; Kim, K.; Yu, K.J. Electronic and Thermal Properties of Graphene and Recent Advances in Graphene Based Electronics Applications. *Nanomaterials* **2019**, *9*, 374. [CrossRef]
27. Cernat, A.; Györfi, S.J.; Irimes, M.-B.; Tertiş, M.; Bodoki, A.; Pralea, I.-E.; Suci, M.; Cristea, C. Click chemistry on azide-functionalized graphene oxide. *Electrochem. Commun.* **2019**, *98*, 23–27. [CrossRef]
28. Rowley-Neale, S.J.; Randviir, E.P.; Abo Dena, A.S.; Banks, C.E. An overview of recent applications of reduced graphene oxide as a basis of electroanalytical sensing platforms. *Appl. Mater. Today* **2018**, *10*, 218–226. [CrossRef]
29. Raicopol, M.D.; Chira, N.A.; Pandele, A.M.; Hanganu, A.; Ivanov, A.A.; Tecuceanu, V.; Bugean, I.G.; Buica, G.-O. Electrodes modified with clickable thiosemicarbazone ligands for sensitive voltammetric detection of Hg(II) ions. *Sens. Actuators B. Chem.* **2020**, *313*, 128030. [CrossRef]
30. Chen, L.; Tang, Y.; Wang, K.; Liu, C.; Luo, S. Direct electrodeposition of reduced graphene oxide on glassy carbon electrode and its electrochemical application. *Electrochem. Commun.* **2011**, *13*, 133–137. [CrossRef]
31. Buica, G.-O.; Ivanov, A.A.; Lazar, I.-G.; Tatu (Arnold), G.-L.; Omocea, C.; Birzan, L.; Ungureanu, E.-M. Colorimetric and voltammetric sensing of mercury ions using 2,2'-(ethane-1,2-diylbis((2-(azulen-2-ylamino)-2-oxoethyl)azanediyl)) diacetic acid. *J. Electroanal. Chem.* **2019**, *849*, 113351. [CrossRef]
32. Buica, G.-O.; Lazar, I.-G.; Saint-Aman, E.; Tecuceanu, V.; Dumitriu, C.; Ivanov, A.A.; Stoian, A.B.; Ungureanu, E.-M. Ultrasensitive modified electrode based on poly(1H-pyrrole-1-hexanoic acid) for Pb(II) detection. *Sens. Actuators B* **2017**, *246*, 434–443. [CrossRef]
33. Water Quality—Determination of Mercury—Method Using Atomic Absorption Spectrometry (AAS) with and without Enrichment. Available online: <https://www.iso.org/standard/51964.html> (accessed on 14 April 2012).
34. Water quality—Determination of Mercury—Method Using Atomic Fluorescence Spectrometry. Available online: <https://www.iso.org/standard/38502.html>. (accessed on 13 June 2006).
35. Salinas, F.; Espinosa-Mansilla, A.; López-Martínez, L.; López-de-Alba, P.L. Selective extraction-spectrophotometric determination of microamounts of palladium in catalysts. *Chem. Anal. (Warsaw)* **2001**, *46*, 239–248.
36. Lobana, T.S.; Sharma, R.; Bawa, G.; Khanna, S. Bonding and structure trends of thiosemicarbazone derivatives of metals—An overview. *Coord. Chem. Rev.* **2009**, *253*, 977–1055. [CrossRef]
37. Padhyé, S.; Kauffman, G.B. Transition metal complexes of semicarbazones and thiosemicarbazones. *Coord. Chem. Rev.* **1985**, *63*, 127–160. [CrossRef]
38. Allongue, P.; Delamar, M.; Desbat, B.; Fagebaume, O.; Hitmi, R.; Pinson, J.; Savéant, J.-M. Covalent Modification of Carbon Surfaces by Aryl Radicals Generated from the Electrochemical Reduction of Diazonium Salts. *J. Am. Chem. Soc.* **1997**, *119*, 201–207. [CrossRef]
39. McCreery, R.L. Advanced Carbon Electrode Materials for Molecular Electrochemistry. *Chem. Rev.* **2008**, *108*, 2646–2687. [CrossRef]
40. Velický, M.; Toth, P.S.; Woods, C.R.; Novoselov, K.S.; Dryfe, R.A.W. Electrochemistry of the Basal Plane versus Edge Plane of Graphite Revisited. *J. Phys. Chem. C* **2019**, *123*, 11677–11685. [CrossRef]

41. Ray, K.; McCreery, R.L. Spatially Resolved Raman Spectroscopy of Carbon Electrode Surfaces: Observations of Structural and Chemical Heterogeneity. *Anal. Chem.* **1997**, *69*, 4680–4687. [[CrossRef](#)]
42. Kariuki, J.K.; McDermott, M.T. Nucleation and Growth of Functionalized Aryl Films on Graphite Electrodes. *Langmuir* **1999**, *15*, 6534–6540. [[CrossRef](#)]
43. Koehler, F.M.; Jacobsen, A.; Ensslin, K.; Stampfer, C.; Stark, W.J. Selective Chemical Modification of Graphene Surfaces: Distinction Between Single- and Bilayer Graphene. *Small* **2010**, *6*, 1125–1130. [[CrossRef](#)]
44. Paulus, G.L.C.; Wang, Q.H.; Strano, M.S. Covalent Electron Transfer Chemistry of Graphene with Diazonium Salts. *Acc. Chem. Res.* **2013**, *46*, 160–170. [[CrossRef](#)] [[PubMed](#)]
45. Hossain, M.Z.; Walsh, M.A.; Hersam, M.C. Scanning Tunneling Microscopy, Spectroscopy, and Nanolithography of Epitaxial Graphene Chemically Modified with Aryl Moieties. *J. Am. Chem. Soc.* **2010**, *132*, 15399–15403. [[CrossRef](#)] [[PubMed](#)]
46. Rice, R.J.; Pontikos, N.M.; McCreery, R.L. Quantitative correlations of heterogeneous electron-transfer kinetics with surface properties of glassy carbon electrodes. *J. Am. Chem. Soc.* **1990**, *112*, 4617–4622. [[CrossRef](#)]
47. Kariuki, J.K.; McDermott, M.T. Formation of Multilayers on Glassy Carbon Electrodes via the Reduction of Diazonium Salts. *Langmuir* **2001**, *17*, 5947–5951. [[CrossRef](#)]
48. Raicopol, M.D.; Andronescu, C.; Atasiei, R.; Hanganu, A.; Vasile, E.; Brezoiu, A.M.; Pilan, L. Organic layers via aryl diazonium electrochemistry: Towards modifying platinum electrodes for interference free glucose biosensors. *Electrochim. Acta* **2016**, *206*, 226–237. [[CrossRef](#)]
49. Bard, A.J.; Faulkner, L.R. *Electrochemical Methods: Fundamentals and Applications*, 2nd ed.; John Wiley & Sons: New York, NY, USA, 2001; p. 237.
50. Matsuda, H.; Ayabe, Y.Z. Zur Theorie der Randles-Sevčičschen Kathodenstrahl-Polarographie. *Elektrochem* **1955**, *59*, 494–503.
51. Nicholson, R.S. Theory and Application of Cyclic Voltammetry for Measurement of Electrode Reaction Kinetics. *Anal. Chem.* **1965**, *37*, 1351–1355. [[CrossRef](#)]
52. Lavagnini, I.; Antiochia, R.; Magno, F. An Extended Method for the Practical Evaluation of the Standard Rate Constant from Cyclic Voltammetric Data. *Electroanalysis* **2004**, *16*, 505–506. [[CrossRef](#)]
53. Cumba, L.R.; Foster, C.W.; Brownson, D.A.C.; Smith, J.P.; Iniesta, J.; Thakur, B.; do Carmo, D.R.; Banks, C.E. Can the mechanical activation (polishing) of screen-printed electrodes enhance their electroanalytical response? *Analyst* **2016**, *141*, 2791–2799. [[CrossRef](#)]
54. Bishop, G.W.; Ahiadu, B.K.; Smith, J.L.; Patterson, J.D. Use of Redox Probes for Characterization of Layer-by-Layer Gold Nanoparticle-Modified Screen-Printed Carbon Electrodes. *J. Electrochem. Soc.* **2017**, *164*, B23–B28. [[CrossRef](#)]
55. Chen, P.; McCreery, R.L. Control of Electron Transfer Kinetics at Glassy Carbon Electrodes by Specific Surface Modification. *Anal. Chem.* **1996**, *68*, 3958–3965. [[CrossRef](#)]
56. Saby, C.; Ortiz, B.; Champagne, G.Y.; Bélanger, D. Electrochemical Modification of Glassy Carbon Electrode Using Aromatic Diazonium Salts. 1. Blocking Effect of 4-Nitrophenyl and 4-Carboxyphenyl Groups. *Langmuir* **1997**, *13*, 6805–6813. [[CrossRef](#)]
57. Greenwood, J.; Phan, T.H.; Fujita, Y.; Li, Z.; Ivasenko, O.; Vanderlinden, W.; Van Gorp, H.; Frederickx, W.; Lu, G.; Tahara, K.; et al. Covalent Modification of Graphene and Graphite Using Diazonium Chemistry: Tunable Grafting and Nanomanipulation. *ACS Nano*. **2015**, *9*, 5520–5535. [[CrossRef](#)]
58. Zhang, Y.; Hao, H.; Wang, L. Effect of morphology and defect density on electron transfer of electrochemically reduced graphene oxide. *Appl. Surf. Sci.* **2016**, *390*, 385–392. [[CrossRef](#)]
59. Barrow, N.J.; Cox, V.C. The effects of pH and chloride concentration on mercury sorption. I. By goethite. *J. Soil. Sci.* **1992**, *43*, 295–304. [[CrossRef](#)]
60. Xu, L.; Yuan, R.; Chai, Y.Q. Mercury(II) ion potentiometric sensor based on a sulfur schiff's base 1-(2-hydroxy-1,2-diphenylethylidene) thiosemicarbazide as ionophore. *Chem. Lett.* **2005**, *34*, 440–441.
61. Ghazy, S.E.-S.; El-Reash, G.M.A.; Al-Gammal, O.A.; Yousef, T. Flotation-separation of toxic metal ions from aqueous solutions using thiosemicarbazide derivatives as chelating agents and oleic acid as a surfactant. *Eur. J. Chem.* **2010**, *1*, 76–82. [[CrossRef](#)]

62. Wang, J. Voltammetry following nonelectrolytic preconcentration. In *Electroanalytical Chemistry: A Series of Advances*; Bard, A.J., Rubinstein, I., Eds.; Marcel Dekker: New York, NY, USA, 1989; Volume 16, pp. 1–89.
63. Taverniers, I.; De Loose, M.; Van Bockstaele, E. Trends in Quality in the Analytical Laboratory. II. Analytical method validation and quality assurance. *Trends Anal. Chem.* **2004**, *23*, 535–552. [[CrossRef](#)]

Publisher's Note: MDPI stays neutral with regard to jurisdictional claims in published maps and institutional affiliations.



© 2020 by the authors. Licensee MDPI, Basel, Switzerland. This article is an open access article distributed under the terms and conditions of the Creative Commons Attribution (CC BY) license (<http://creativecommons.org/licenses/by/4.0/>).